ELSEVIER

Journal of Quantitative Spectroscopy & Radiative Transfer 99 (2006) 327–340

Journal of Quantitative Spectroscopy & Radiative Transfer

www.elsevier.com/locate/jqsrt

Optical properties of plasmas based on an average-atom model

W.R. Johnson[a,*], C. Guet[b], G.F. Bertsch[c]

[a]*Department of Physics, University of Notre Dame, 225 Nieuwland Science Hall, Notre Dame, IN 46556, USA*
[b]*CEA/DAM Ile de France, BP12, 91680 Bruyères-le-Châtel, France*
[c]*Department of Physics and Institute of Nuclear Theory, University of Washington, Box 351560, Seattle, WA 98915, USA*

Accepted 26 April 2005

Abstract

Optical properties of plasmas, including dielectric constants, indices of refraction, and absorption coefficients, are determined from an average-atom point of view. Linear response of an average atom to a harmonic electric field leads to an average-atom version of the Kubo–Greenwood formula, which is used to calculate the frequency-dependent electric conductivity of the plasma. The frequency-dependent dielectric function is determined from the conductivity using Kramers–Kronig dispersion relations. The index of refraction and absorption coefficient of the plasma are subsequently obtained from the dielectric function. Comparing the present results with the free-electron model helps one understand anomalies observed recently in space and time resolved interferograms of Al plasmas produced by 13.9- and 14.7-nm X-ray lasers.

PACS: 51.70.+f; 52.25.Mq; 32.70.Cs; 32.80.Fb

Keywords: Plasma; Conductivity; Dielectric function; Index of refraction; Dispersion relations; X-ray interferometry

1. Introduction

X-ray interferograms are widely used in plasma diagnostics owing to the fact that they can be interpreted in terms of the index of refraction n, from which the electron density can be

*Corresponding author.
E-mail address: johnson@nd.edu (W.R. Johnson).

0022-4073/$ - see front matter
doi:10.1016/j.jqsrt.2005.05.026

determined. The free-electron model, which is frequently used to interpret the index of refraction, predicts that $n<1$. Recently, however, instances where $n>1$ have been observed in interferograms of an Al plasma produced by a 14.7-nm Ni-like Pd soft X-ray laser at the Lawrence Livermore National Laboratory COMET laser facility [1]. Similar anomalies were noted in interference patterns of an Al plasma produced by a 13.9-nm Ni-like Ag laser at the Advanced Photon Research Center of the Japan Atomic Energy Research Institute [2]. These anomalies have been attributed to the influence of bound electrons on the optical properties of the plasma [1–3].

In the present work, we study optical properties of plasmas theoretically starting from an average-atom cell model and confirm that at low temperatures (1–4 eV) the index of refraction of a dense Al plasma is indeed greater than 1 for photon wavelengths in the range 10–15 nm. Our average-atom model is a quantum-mechanical version of the generalized Thomas–Fermi model of a plasma devised more than a half-century ago by Feynman et al. [4] and is similar to a model used previously by Blenski and Ishikawa [5]. Applying linear response theory to the average atom leads to a version of the Kubo–Greenwood (KG) formula [6–10] for the frequency-dependent conductivity $\sigma(\omega)$ of the plasma. It should be noted that the KG formula has also been used recently in Refs. [11,12] to study plasma conductivity from a molecular dynamics point of view. Conductivity is related to the imaginary part of the relative dielectric function $\varepsilon_r(\omega)$; therefore, with the aid of Kramers–Kronig dispersion relations [13–16], one can determine the entire complex dielectric function $\varepsilon_r(\omega)$ and the corresponding complex index of refraction $n(\omega)+\mathrm{i}\kappa(\omega)=\sqrt{\varepsilon_r(\omega)}$.

In the following sections, we outline the average-atom model, derive the KG formula, and use a dispersion relation to obtain the dielectric function. Finally, we apply the model to evaluate the index of refraction and absorption coefficient of an aluminum plasma (density 10^{20} ions/cc) in a temperature range $T=1-30$ eV. These results are compared with the free-electron model in an effort to explain the anomalies discussed above.

2. Quantum-mechanical average-atom model

The plasma is divided into neutral cells, each containing Z electrons, centered on a nucleus of charge Z. The radius of each cell is taken to be the Wigner–Seitz (WS) radius, determined from the density and atomic weight. Each electron is assumed to satisfy the self-consistent central-field Schrödinger equation

$$\left[\frac{p^2}{2m}-\frac{Z}{r}+V\right]u_a(\boldsymbol{r})=\varepsilon u_a(\boldsymbol{r}), \tag{1}$$

where $a=(n,l)$ for bound states or (ε,l) for continuum states. The potential inside a cell consists of two parts: $V(r)=V_{\mathrm{dir}}+V_{\mathrm{exc}}$. Outside the cell $V=0$. The direct part of the potential is obtained from

$$\nabla^2 V_{\mathrm{dir}}=-4\pi\rho, \tag{2}$$

where the electron density $\rho=\rho_b+\rho_{\mathrm{c}}$ has contributions from both bound and continuum electrons. In the present work, the exchange potential is given by the local

density approximation

$$V_{\rm exc} = -\left(\frac{3}{\pi}\rho(r)\right)^{1/3}. \tag{3}$$

The exchange potential could, of course, be replaced by a more realistic exchange-correlation potential such as that given in [17] or [18].

The bound-state contribution to the density is

$$4\pi r^2 \rho_b(r) = \sum_{nl} 2(2l+1) f_{nl} P_{nl}(r)^2, \tag{4}$$

where $P_{nl}(r)$ is the bound-state radial wave function,

$$f_{nl} = \frac{1}{1+\exp[(\varepsilon_{nl}-\mu)/kT]}$$

is the Fermi distribution function for a state with quantum numbers (nl), μ is the chemical potential, and T is the temperature. The summation in Eq. (4) ranges over all subshells. Contributions to the density from continuum electrons $\rho_{\rm c}$ are given by a similar formula with the bound-state radial function $P_{nl}(r)$ replaced by the continuum wave function $P_{\varepsilon l}(r)$ normalized on the energy scale and the sum over n replaced by an integral over ε. To accelerate convergence of the sum over l in the continuum case, we follow the suggestion in Ref. [5] and subtract the free-particle contribution from each partial wave, then add back the exactly known free-particle density.

Finally, the chemical potential μ is chosen to ensure electric neutrality of the Wigner–Seitz cell:

$$Z = \int_{r<R} \rho(r)\,{\rm d}^3 r \equiv \int_0^R 4\pi r^2 \rho(r)\,{\rm d}r. \tag{5}$$

Eqs. (1–5) are solved self-consistently to give the chemical potential μ, the electrostatic potential $V(r)$, and the electron density $\rho(r)$.

2.1. Example: Al at $T = 5\,eV$ and density $0.27\,gm/cc$

As an illustration of the present average-atom model, consider aluminum at $0.1\times$ metallic density and $T = 5\,{\rm eV}$. The corresponding WS radius is $R = 6.44\,{\rm a.u.}$ The average-atom potential in this case supports five bound states; their energies and the associated number of electrons $n(l)$ inside the Wigner–Seitz cell are given in Table 1. For each continuum partial wave, we list $n(l)$, $n_0(l)$ the number of "free" waves within the cell, and differences $\Delta n(l) = n(l) - n_0(l)$, which are seen to converge more rapidly at large l. Note that $N_{\rm bound} + N_{\rm free} = 13$ for overall charge neutrality.

In the left panel of Fig. 1, we show bound and continuum contributions to the radial density for the case described in Table 1, and in the right panel the continuum contribution to the electron density $\rho_{\rm c}(r)$ is compared with the free-electron background density ρ_0. The density merges smoothly into the background outside the Wigner–Seitz sphere.

Table 1
Average atom of aluminum at density 0.27 gm/cc and temperature $T = 5\,\mathrm{eV}$

Bound states			l	Continuum states		
State	Energy	$n(l)$		$n(l)$	$n_0(l)$	$\Delta n(l)$
1s	−55.189	2.0000	0	0.1090	0.1975	−0.0885
2s	−3.980	2.0000	1	0.2149	0.3513	−0.1364
3s	−0.259	0.6759	2	0.6031	0.3192	0.2839
2p	−2.610	6.0000	3	0.2892	0.2232	0.0660
3p	−0.054	0.8300	4	0.1514	0.1313	0.0201
			5	0.0735	0.0674	0.0061
			6	0.0326	0.0308	0.0018
			7	0.0132	0.0127	0.0005
			8	0.0049	0.0048	0.0001
			9	0.0017	0.0016	0.0001
			10	0.0005	0.0005	0.0000
Nbound		11.5059	Nfree	1.4941	1.3404	0.1537

The Wigner–Seitz radius is $R = 6.44\,\mathrm{a.u.}$ and the chemical potential is $\mu = -0.3823\,\mathrm{a.u.}$ Five bound states are found. The number of electrons contained within the Wigner–Seitz cell $n(l)$ are also listed.

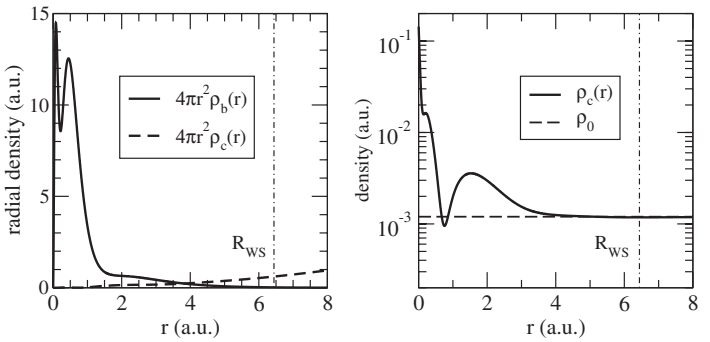

Fig. 1. Left panel: Bound and continuum contributions to the radial electron densities for Al at $T = 5\,\mathrm{eV}$ and density 0.27 gm/cc. Right panel: Continuum contribution to the electron density $\rho_c(r)$ merges smoothly into the background density ρ_0.

3. Linear response and the Kubo–Greenwood formula

We assume that a time-dependent electric field is applied to an average atom. We describe the field by the vector potential

$$\boldsymbol{A}(t) = \frac{F}{\omega}\hat{\boldsymbol{z}}\cos\omega t.$$

The one-electron Hamiltonian is

$$H = \frac{1}{2m}[p_x^2 + p_y^2 + (p_z - eA_z(t))^2] + V(n,r) = T + V(n,r) - \frac{eF}{\omega} v_z \cos\omega t, \tag{6}$$

where we have retained only those terms linear in the field strength F. The time-dependent Schrödinger equation becomes

$$\left[T_0 + V(n,r) - \frac{eF}{\omega} v_z \cos\omega t\right]\psi_i(\boldsymbol{r},t) = \mathrm{i}\,\frac{\partial}{\partial t}\,\psi_i(\boldsymbol{r},t). \tag{7}$$

We seek a solution to Eq. (7) of the form

$$\psi_i(\boldsymbol{r},t) = u_i(\boldsymbol{r})\mathrm{e}^{-\mathrm{i}\varepsilon_i t} + w_i^+(\boldsymbol{r})\mathrm{e}^{-\mathrm{i}(\varepsilon_i+\omega)t} + w_i^-(\boldsymbol{r})\mathrm{e}^{-\mathrm{i}(\varepsilon_i-\omega)t},$$

where $u_i(\boldsymbol{r})$ is a solution to the time-independent Schrödinger equation and where $w_i^{\pm}(\boldsymbol{r})$ are small perturbations. We find

$$[T_0 + V(n,r)]u_i(\boldsymbol{r}) = \varepsilon_i u_i(\boldsymbol{r}), \tag{8}$$

$$[T_0 + V(n,r) - (\varepsilon_i \pm \omega)]w_i^{\pm}(\boldsymbol{r}) = \frac{eF}{2\omega}\, v_z u_i(\boldsymbol{r}). \tag{9}$$

In writing these equations, we have ignored the modifications of the potential $V(n,r)$ induced by the field. Taking these into account would lead to an average-atom version of the random-phase approximation [19].

Next, we carry out an eigenvalue expansion of the perturbed orbital as

$$w_i^+(\boldsymbol{r}) = \sum_j X_i^j u_j(\boldsymbol{r}), \quad w_i^-(\boldsymbol{r}) = \sum_j Y_i^j u_j(\boldsymbol{r}).$$

From (9), we find

$$X_i^j = \frac{eF}{2\omega}\frac{\langle j|v_z|i\rangle}{\varepsilon_j - i\eta - \varepsilon_i - \omega}, \quad Y_i^j = \frac{eF}{2\omega}\frac{\langle j|v_z|i\rangle}{\varepsilon_j - i\eta - \varepsilon_i + \omega}.$$

The current associated with the perturbed atom is

$$\begin{aligned} J_z(t) &= \frac{2e}{\Omega}\sum_i f_i\langle\psi_i(t)|v_z|\psi_i(t)\rangle \\ &= \frac{2e}{\Omega}\sum_i f_i[(\langle u_i|v_z|w_i^+\rangle + \langle w_i^-|v_z|u_i\rangle)\mathrm{e}^{-\mathrm{i}\omega t} + \text{c.c.}], \end{aligned} \tag{10}$$

to terms linear in F. In the above equation Ω is the volume/atom. The Fermi distribution function f_i for state i accounts for the initial state occupation in the average atom and the factor of 2 in Eq. (10) accounts for two spin states/electron.

The response current may be rewritten in terms of the expansion coefficients as

$$J = \frac{2e}{\Omega}\sum_{ij} f_i[(\langle i|v_z|j\rangle X_i^j + \langle j|v_z|i\rangle\, Y_i^{j\star})\mathrm{e}^{-\mathrm{i}\omega t} + \text{c.c.}]. \tag{11}$$

The conductivity is determined by the part of the current J_1 in phase with the driving field:

$$J_1 = \frac{4e}{\Omega}\sum_{ij} f_i \Im(\langle i|v_z|j\rangle X_i^j + \langle j|v_z|i\rangle Y_i^{j\star}) \sin\omega t.$$

One finds

$$\Im(\langle i|v_z|j\rangle X_i^j + \langle j|v_z|i\rangle Y_i^{j\star}) = \frac{eF}{2\omega}\sum_j (\pi\delta(\varepsilon_j - \varepsilon_i - \omega)|\langle i|v_z|j\rangle|^2 - \pi\delta(\varepsilon_j - \varepsilon_i + \omega)|\langle j|v_z|i\rangle|^2). \tag{12}$$

Interchanging indices $i \leftrightarrow j$ in the second term leads to $J_1(t) = \sigma(\omega)E_z(t)$ with

$$\sigma(\omega) = \frac{2\pi e^2}{\omega\Omega}\sum_{ij}(f_i - f_j)\ |\langle j|v_z|i\rangle|^2\delta(\varepsilon_j - \varepsilon_i - \omega), \tag{13}$$

which is an average-atom version of the KG formula.

3.1. Reduction of the Kubo–Greenwood formula

There are three distinct contributions to Eq. (13) arising from free–free transitions, bound–bound transitions (line spectrum) and from bound–free transitions (photoabsorption).

3.1.1. Free–free

The free–free (inverse bremsstrahlung) contribution to the conductivity which dominates near $\omega = 0$ where other channels are closed is given by

$$\sigma(\omega) = \frac{2\pi e^2}{3\omega\Omega}\sum_{l_i}\int_0^\infty \mathrm{d}\varepsilon_i (f_i - f_j)[|\langle\varepsilon_i l_i\|v\|\varepsilon_j l_i + 1\rangle|^2 + |\langle\varepsilon_i l_i\|v\|\varepsilon_j l_i - 1\rangle|^2], \tag{14}$$

with $\varepsilon_j = \varepsilon_i + \omega$.

Sample matrix elements for a test case with $\varepsilon_i = 1$ a.u. and $l_i = 2$ are shown in Fig. 2 as functions of ω, where $\omega = \varepsilon_f - \varepsilon_i$.

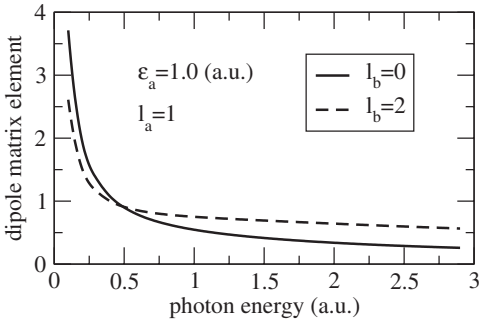

Fig. 2. Test radial matrix elements $\langle\varepsilon_a l_a\|v\|\varepsilon_a + \omega l_b\rangle$ for an average atom of Al (5 eV and 0.1 metallic density) are given as functions ω. The initial energy ε_a is 1 a.u. and the initial angular momentum $l_a = 1$.

It is apparent from the figure that the radial matrix elements diverge as ω^{-1} for small ω. This behavior is a consequence of the fact that we have ignored interactions of electrons with ions outside the WS cell in our average-atom model.

Owing to the infrared divergence in radial matrix elements, the conductivity diverges as $1/\omega^2$. This low-frequency divergence would be protected in more sophisticated calculations by finite lifetimes of excited states. In the present calculation, we mock up such contributions using a scaling factor $\omega^2/(\gamma^2+\omega^2)$ in the integrand of the KG formula to remove the divergence. The resulting conductivity behaves as

$$\sigma(\omega) \approx \frac{\sigma(0)\gamma^2}{\gamma^2+\omega^2}$$

for small ω, in harmony with the classical Drude model [20,21] of conductivity. In the classical model of conductivity, γ is the mean electron–ion collision rate. In the present work, the scaling factor γ is chosen in such a way that the free–free contribution to the conductivity sum rule,

$$\int_0^\infty \sigma(\omega)\,\mathrm{d}\omega = \frac{\pi}{2}\frac{e^2 N_{\mathrm{free}}}{m\Omega}, \tag{15}$$

is satisfied. Here N_{free} is the number of free electrons/ion and Ω is the Wigner–Seitz cell volume or, equivalently, the volume/ion.

For the example of Al at $T = 5\,\mathrm{eV}$ and density 0.27 gm/cc discussed in the previous section, the number of free electrons/ion is 1.494 leading to $\gamma = 0.0466\,\mathrm{a.u.} = 1.27\,\mathrm{eV}$. The limiting value of the conductivity in this case is $\sigma(0) = 0.0262\,\mathrm{a.u.} = 0.121\,(\mu\Omega - \mathrm{m})^{-1}$. It should be noted that scaling has no effect for $\omega \gg \gamma$. Results of evaluating Eq. (14) with scaling are shown in the lower left panel of Fig. 3. The static conductivity obtained from the Ziman formula [22, Chapter 8] for the example of Al at $T = 5\,\mathrm{eV}$ and density 0.27 gm/cc is $\sigma_{\mathrm{Ziman}} = 0.125\,(\mu\Omega - \mathrm{m})^{-1}$ in good agreement with the present value.

3.1.2. Bound–bound

The contribution to the conductivity from bound–bound transitions is

$$\sigma(\omega) = \frac{2\pi e^2}{3\Omega}\sum_{n_i l_i n_j l_j}\frac{(f_i - f_j)}{\omega_{ij}}\,|\langle n_i l_i \| v \| n_j l_j\rangle|^2, \tag{16}$$

where $\omega_{ij} = \varepsilon_j - \varepsilon_i > 0$. This leads to a finite number of discrete line contributions.

To give a specific example, we return to the case of Al at density 0.27 gm/cc and $T = 5\,\mathrm{eV}$. Four transitions listed in Table 2 contribute to the conductivity. Two other possibilities permitted by dipole selection rules (1s $\to$ 2p and 2s $\to$ 2p) do not contribute since $n = 1$ and $n = 2$ states are completely occupied in this example. Three of the four bound–bound transitions are also illustrated in the upper left panel of Fig. 3, where we have folded the lines into a Lorentzian line profile of width γ given by the effective collision rate discussed in the previous subsection. The effective number of electrons contributing to the bound–bound part of the conductivity sum rule in this example is $N_{\mathrm{bb}} = 0.493$.

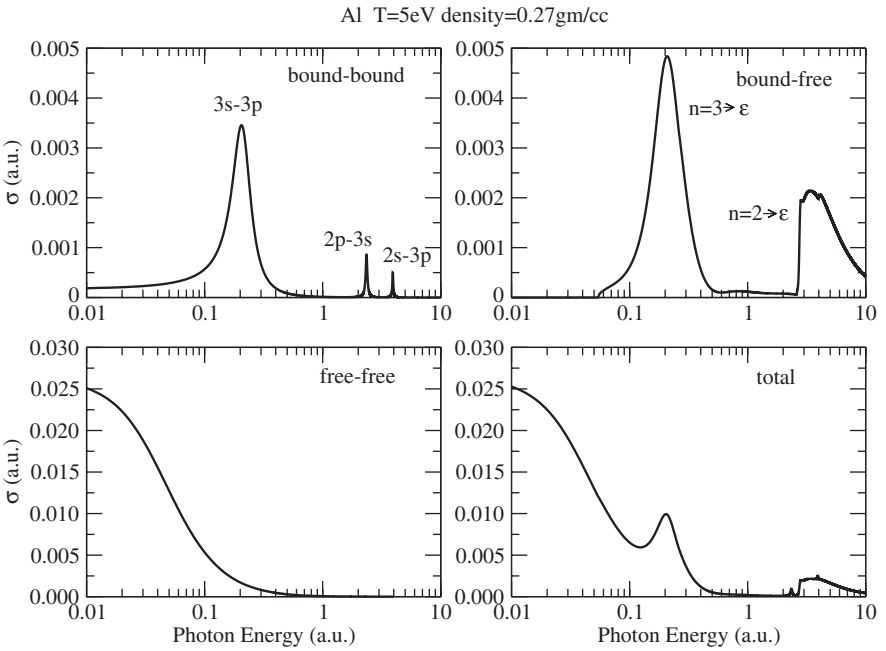

Fig. 3. Contributions to the conductivity for an average atom of Al (5 eV and 1/10 metallic density) is given as functions of the photon energy. Upper left: bound–bound. Upper right: bound–free. Lower left: free–free. Lower right: total $\sigma(\omega)$.

Table 2
Bound–bound contributions to the conductivity for Al at $T = 5$ eV and density 0.27 gm/cc

$i \to j$	ω_{ij}	$\sigma(\omega_{ij})$
3s → 3p	0.205	0.0004702
2p → 3s	2.350	0.0001248
2s → 3p	3.926	0.0000726
1s → 3p	55.135	0.0000239
Sum		0.0006914

3.1.3. Bound–free

The contribution to the Kubo formula from bound–free (photoionization) channels is

$$\sigma(\omega) = \frac{2\pi e^2}{3\omega\Omega}\sum_{n_i l_i}(f_i - f_j)[|\langle n_i l_i \| v \| \varepsilon_j l_i + 1\rangle|^2 + |\langle n_i l_i \| v \| \varepsilon_j l_i - 1\rangle|^2], \tag{17}$$

where $\varepsilon_j = \varepsilon_i + \omega$. For each occupied subshell $n_i l_i$ there are contributions for all $\omega > -\varepsilon_i$.

In Fig. 3 we show the contribution to the conductivity given by Eq. (17) for our example of an average atom at density 0.27 gm/cc and $T = 5\,\mathrm{eV}$. The prominent low-energy peak is associated with ionization of the partially occupied 3p and 3s subshells. The irregular shoulder near 3 a.u. is caused by the opening of the 2p and 2s ionization channels. The contribution to the conductivity from the 1s shell, which is ionized at 55 a.u., is not shown in the figure. The sum of the three contributions discussed above is shown in the lower right panel of Fig. 3.

4. Dispersion relations

The complex dielectric function is related to the complex conductivity through the relation

$$\varepsilon_r(\omega) = 1 + \mathrm{i}\,\frac{4\pi\sigma(\omega)}{\omega}. \tag{18}$$

Thus the imaginary part of the dielectric function is defined once the real part of the conductivity is given by the KG formula,

$$\Im\varepsilon_r(\omega) = \frac{4\pi}{\omega}\,\Re\sigma(\omega). \tag{19}$$

On the general grounds of causality, one may infer the real part of the dielectric function from its imaginary part using the Kramers–Kronig dispersion relations [13–16]. In turn, Eq. (18) provides the imaginary part of the conductivity. It follows that the real and imaginary parts of the complex conductivity also satisfy a dispersion relation,

$$\Im\sigma(\omega_0) = -\frac{2\omega_0}{\pi}\fint_0^\infty \frac{\Re\sigma(\omega)}{\omega^2-\omega_0^2}\,\mathrm{d}\omega. \tag{20}$$

In the high frequency limit, the dispersion relation given in Eq. (20) takes the form

$$\Im\sigma(\omega_0) \to \frac{2}{\pi}\frac{1}{\omega_0}\int_0^\infty \Re\sigma(\omega)\,\mathrm{d}\omega. \tag{21}$$

In virtue of the conductivity sum rule used earlier, Eq. (21) shows that $\Im\sigma(\omega)$ has the limiting value $n_e e^2/(m\omega_0)$, in harmony with the free-electron limit of the dielectric function

$$\varepsilon_r \to 1 - \frac{4\pi n_e e^2}{m\omega^2}. \tag{22}$$

Let us apply the dispersion relation (20) to the example of Al at density 0.27 gm/cc and $T = 5\,\mathrm{eV}$ discussed in the previous section. In Fig. 4, we show $\Re\sigma(\omega)$ from the earlier KG analysis as dashed curve and we show $\Im\sigma(\omega)$ from the dispersion relation (20) as solid curves.

With the aid of Eq. (18), we can reconstruct the complex dielectric function in terms of these two functions and completely describe the optical properties of the plasma.

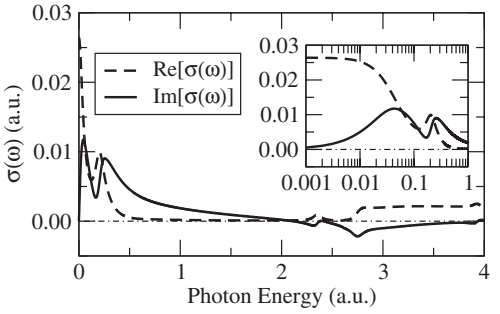

Fig. 4. Real part of $\sigma(\omega)$ (dashed lines) and imaginary parts of $\sigma(\omega)$ (solid lines) for Al at 5 eV and density 0.27 a.u.

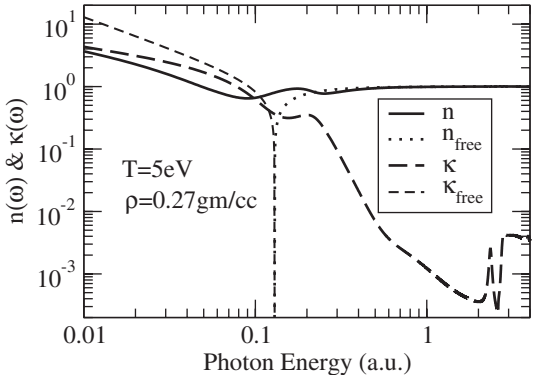

Fig. 5. Real $n(\omega)$ and imaginary $\kappa(\omega)$ parts of the index of refraction for an average atom of Al (5 eV and 1/10 metallic density) given as functions of the photon energy ω. The lightly dashed and dotted lines give n and κ in the free-electron approximation. The singularity in the free-electron case occurs at the plasma frequency.

4.1. Index of refraction

The real and imaginary parts of the relative dielectric function $\varepsilon(\omega)$ are given by Eq. (18), which in atomic units reduce to

$$\Re\varepsilon_r(\omega) = 1 - 4\pi\frac{\Im\sigma(\omega)}{\omega}, \quad \Im\varepsilon_r(\omega) = 4\pi\frac{\Re\sigma(\omega)}{\omega}.$$

The complex index of refraction $n + \mathrm{i}\kappa$ is related to $\varepsilon(\omega)$ through the equation

$$n + \mathrm{i}\kappa = \sqrt{\varepsilon_r}.$$

It follows that

$$n(\omega) = \sqrt{\frac{\sqrt{[\Re\varepsilon_r(\omega)]^2 + [\Im\varepsilon_r(\omega)]^2} + \Re\varepsilon_r(\omega)}{2}}, \tag{23}$$

$$\kappa(\omega) = \sqrt{\frac{\sqrt{[\Re\varepsilon_r(\omega)]^2 + [\Im\varepsilon_r(\omega)]^2} - \Re\varepsilon_r(\omega)}{2}}. \tag{24}$$

The two functions $n(\omega)$ and $\kappa(\omega)$ are illustrated in Fig. 5, where they are plotted for the example of Al at $T = 5\,\mathrm{eV}$ and density 0.27 gm/cc.

5. Application to an Al plasma

As mentioned in the introduction, the analysis of interferograms produced by 13.9- and 14.7-nm X-ray lasers gave a plasma index of refraction $n > 1$ in some instances. When analyzed in terms of the free-electron model this leads to the conclusion that the square of the plasma frequency ω_0^2, which is proportional to number of free electrons per ion, is negative in the few eV temperature range. In [2] this behavior was attributed to the 2p–3d transition in Al^{+2}. To examine this anomalous behavior in terms of the average-atom model, we compare $n(\omega) - 1$ predicted by the average-atom model with its free-electron counterpart $n_{\mathrm{free}}(\omega) - 1 \approx -\omega_0^2/(2\omega^2)$.

In the lower panel of Fig. 6, we plot the ratio $(n-1)/(n_{\mathrm{free}} - 1)$ over the range of photon energies $\omega = 0$–$100\,\mathrm{eV}$ for temperature $T = 3\,\mathrm{eV}$. The number of free electrons per ion from the average-atom model is $\langle Z\rangle = 1.38$ for this density and temperature. As can be seen in the figure,

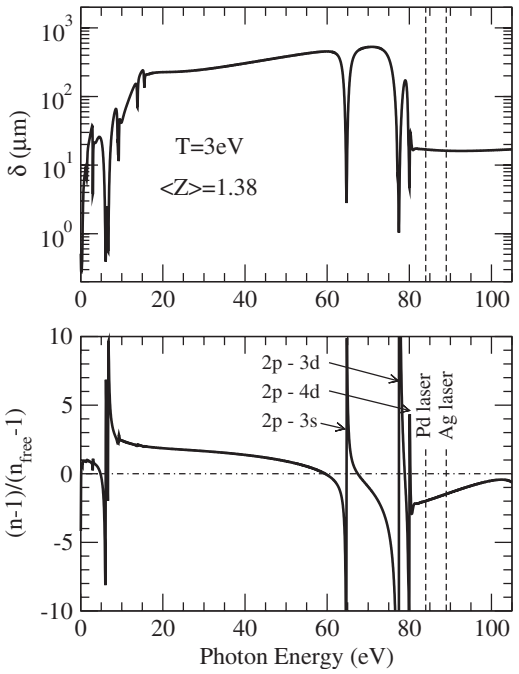

Fig. 6. Lower panel: Ratio of $(n-1)$, calculated in the average-atom model, to $(n_{\mathrm{free}} - 1)$ for an Al plasma at temperature $T = 3\,\mathrm{eV}$ and ion density 10^{20}/cc. The number of free electrons/ion is $\langle Z\rangle = 1.38$. Upper panel: Penetration depth δ (μm) for the same case.

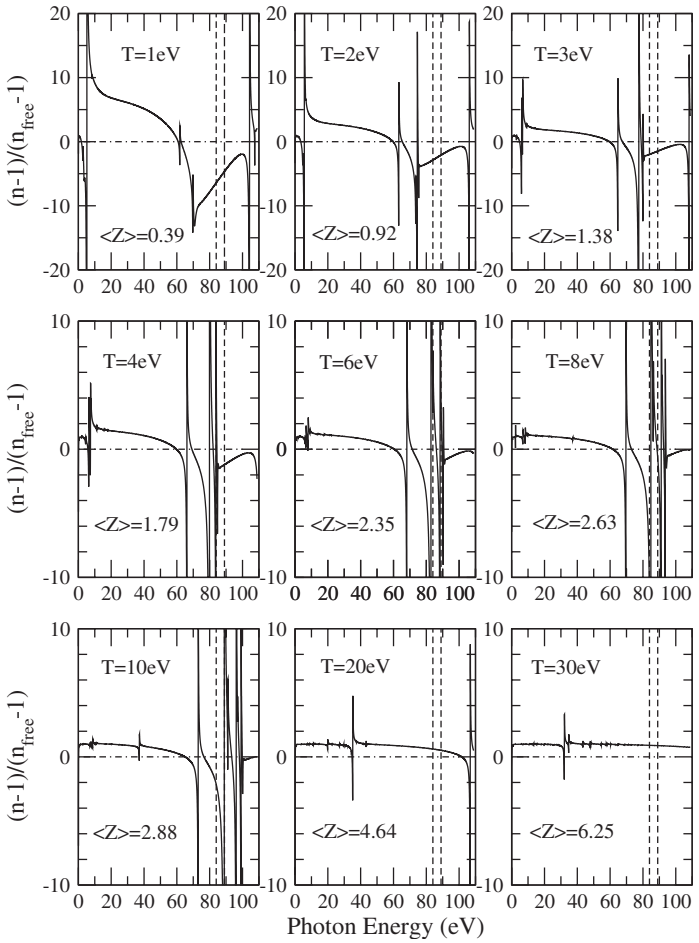

Fig. 7. Ratios $(n-1)/(n_{\mathrm{free}}-1)$ in the average-atom model for Al plasmas with temperatures in the range [1–30] eV and ion density 10^{20}/cc. Dashed vertical lines mark energies of 14.7- and 13.9-nm lasers.

the ratio is near -2 in a band of photon energies that include those of the Pd and Ag lasers indicated by the dashed lines at 84 and 89 eV. This explains the behavior seen experimentally; the main effect on the dispersion integral in this region comes from 2p–2s and 2p–3d transitions and from photoionization of the 2p subshell (threshold at 80.2 eV). In the upper panel of Fig. 6, we plot the penetration depth $\delta = 2c/(\omega\kappa)$ for the case above example. In the range of experimental interest, the average-atom model predicts $\delta \approx 15\,\mu$m.

In Fig. 7, we present ratios $(n-1)/(n_{\mathrm{free}}-1)$ for an Al plasma of density 10^{20} ions/cc and temperatures ranging from 1–30 eV. For $T<4$ eV, the ratio is negative for photon energies in the range of experimental interest. For $4<T<15$ eV, resonances associated with transitions from the $n=2$ shell cross the region of interest, while for $T>20$ eV the ratio is close to 1 over the entire region.

6. Conclusion

We have introduced an average-atom model, fashioned after the generalized Thomas–Fermi model of Feynman et al. [4], and used the model to investigate the optical properties of plasmas. Linear response of the average atom leads to a version of the Kubo–Greenwood formula for the frequency-dependent conductivity $\sigma(\omega)$, which is simply related to the imaginary part of the relative dielectric function. Analytic properties of the dielectric function permit us to determine the real part of the dielectric function from its imaginary part through a dispersion integral. With the complex dielectric function in hand, we can investigate various optical properties of the plasma. As a specific application of the theory, we consider the index of refraction of an Al plasma, density 10^{20} ions/cc, in the temperature range $T = 1$–30 eV. At the lower end of this range, the model predicts that the index of refraction is greater than 1, in harmony with recent observations [1,2], while at the upper end, $n - 1$ from the average-atom model agrees well with the value obtained from a free-electron analysis. Use of the free-electron model to extract electron densities from interferometric data clearly requires some preliminary study to determine whether or not bound–bound resonances and/or photoionization thresholds contribute significantly to the index of refraction. The present extension of the average-atom model provides a useful tool for investigating such questions.

Acknowledgements

The work of WRJ was supported in part by NSF Grant no. PHY-01-39928 and in part by Grant no. B516165 from Lawrence Livermore National Laboratory. The authors wish to thank J. Nilsen for bringing the X-ray laser interferometry experiments to their attention. Debts of thanks are also owed to J.J. Niez for explaining how to evaluate free–free matrix elements of the velocity operator in terms of Lommel integrals and to Michael Kuchiev for discussions concerning the infrared divergence of the conductivity in the average-atom model.

References

[1] Filevich J, Rocca JJ, Marconi MC, Smith RF, Dunn J, Keenan R, et al. Evidence of bound electron contributions to soft X-ray interferograms of dense plasmas. In: X-ray lasers 2004: proceedings of the 9th international conference on X-ray lasers, 2004.
[2] Tang H, Guilbaud O, Jamelot G, Ros D, Klisnik A, Joyeux D, et al. Diagnostics of laser-induced plasma with soft X-ray (13.9 nm) bi-mirror interference microscopy. Appl Phys B 2004;78:975–7.
[3] Nilsen J, Scofield JH. Plasmas with index of refraction greater than one. Opt Lett 2004;29:2677–9.
[4] Feynman RP, Metropolis N, Teller E. Equations of state of elements based on the generalized Fermi–Thomas theory. Phys Rev 1949;75:1561.
[5] Blenski T, Ishikawa K. Pressure ionization in the spherical ion-cell model of dense-plasmas and a pressure formula in the relativistic Pauli approximation. Phys Rev E 1995;51:4869–81.
[6] Kubo R. A general expression for the conductivity tensor. Canad J Phys 1956;34:1274.
[7] Kubo R. Statistical-mechanical theory of irreversible processes I General theory and simple applications to magnetic and conduction problems. J Phys Soc Jpn 1957;12:570.

[8] Greenwood DA. The Boltzmann equation in the theory of electrical conduction in metals. Proc Phys Soc London 1958;715:585.
[9] Harrison WA. Solid state theory. New York: McGraw-Hill; 1970.
[10] Ashcroft NW, Mermin ND. Solid-state physics. Philadelphia: Saunders; 1976.
[11] Desjarlais MP, Kress JD, Collins LA. Electrical conductivity for warm, dense aluminum plasmas and liquids. Phys Rev E 2002;66:025401(R).
[12] Recoules V, Renaudin P, Cléouin J, Noiret P, Zérah G. Electrical conductivity of hot expanded aluminum: experimental measurements and ab initio calculations. Phys Rev E 2002;66:056412.
[13] Kronig RdeL. On the theory of dispersion of X-rays. J Opt Soc Am 1926;12:547.
[14] Kramers HA. Some remarks of the theory of absorption and refraction of X-rays. Nature 1926;117:775.
[15] Kronig RdeL, Kramers HA. La diffusion de la lumière par les atomes. Atti Congr Intern Fisici 1927;2:545.
[16] Landau LD, Lifshitz EM. Electrodynamics of continuous media. New York: Pergamon; 1984.
[17] Gunnarsson O, Lundqvist BI. Exchange and correlation in atoms, molecules, and solids by spin-density functional formalism. Phys Rev B 1976;13:4274–98.
[18] Perdew JP, Zunger A. Self-interaction correction to density-functional approximations for many-electron systems. Phys Rev B 1981;23:5048–79.
[19] Csanak G, Kilcrease DP, Meneses GD. Coupled channel formulation of the perturbed finite-temperature atomic random phase approximation: single channel approximation. JQSRT 2003;81:247–54.
[20] Drude PKL. Zur electronentheorie I. Ann Phys 1900;1:566–613.
[21] Drude PKL. Zur electronentheorie II. Ann Phys 1900;3:369–402.
[22] Mahan GD. Many-particle physics, 3rd ed. New York: Plenum Press; 2000.